RSC Advances

PAPER

View Article Online
View Journal | View Issue

Cite this: *RSC Adv.*, 2020, **10**, 38578

A smart use of biomass derivatives to template an *ad hoc* hierarchical SAPO-5 acid catalyst†

Francesco Mariatti,[a] Ivana Miletto,[b] Geo Paul,[b] Leonardo Marchese,[b] Silvia Tabasso,[c] Maela Manzoli,[a] Giancarlo Cravotto[a] and Enrica Gianotti*[b]

Received 21st July 2020
Accepted 1st October 2020

DOI: 10.1039/d0ra06353c

rsc.li/rsc-advances

A smart design of hierarchical SAPO-5 acid catalyst using biomass derived monosaccharides as sustainable and low-cost mesoporogens has been developed. The hierarchical SAPO-5 was characterized by several physico-chemical techniques to elucidate structure–properties relationships and was tested as a catalyst in the MW-assisted glucose transformation in 5-HMF using γ-valerolactone (GVL) as green solvent.

Zeolites and related microporous solids are well known heterogeneous acid catalysts for oil refining, petrochemistry, pollution abatement and synthesis of fine chemicals.[1,2] One recently emerging field of zeolite application is in biomass valorization processes to produce biofuels, platform molecules and bio-based chemicals.[3–5] Due to the biomass chemical complexity, the development of novel approaches to synthesize zeolites or zeo-type materials with tailored properties towards clean, selective and efficient processes for biomass conversion is nowadays a great challenge for the scientific community.

The tunability of Brønsted/Lewis acidity in a zeolite framework is an important parameter that will affect significantly the catalytic activity and selectivity in biomass upgrading. Moreover, because biomass is made of different kinds of large molecules (mainly polysaccharides, disaccharides and lignin), the accessibility of the acid active sites is a key parameter to avoid mass transfer constraints. In fact, zeolites and zeo-type systems impose diffusion limitation due to the presence of micropores and expedite catalyst deactivation through coke deposition.[6] To circumvent this drawback, hierarchical porous zeolites have been developed, following top-down or bottom-up synthetic approaches, to combine the microporous structure with an additional mesoporous network to improve mass transport to the internal active sites.[7,8]

Among zeolite-type materials, the silicoaluminophosphates (SAPOs) represent a viable alternative to aluminosilicates for applications requiring acid catalysis.[9,10] In particular, SAPO-5 (AFI framework type) is a well known microporous acid catalyst with one-dimensional 12-ring channels (7.3 Å × 7.3 Å).[10,11] In this communication, hierarchical SAPO-5 has been synthetized by a bottom-up approach using a mixture of monosaccharides obtained after the microwave (MW)-assisted conversion of a residual biomass (MsB). The aim was to design the pore architecture of the hierarchical SAPO-5 catalyst, which was tested in the MW-assisted conversion of a model sugar structure (glucose) into 5-(hydroxymethyl)furfural (5-HMF). Glucose was chosen as benchmark substrate because of its similarity with the employed biomass-derived sugar templates. According to this smart approach, MsB have been used as sustainable and low-cost mesoporogens for the preparation of hierarchical porous materials,[12,13] avoiding the use of sophisticated and expensive templates. Indeed, the mixture of MsB used to template the inorganic structure was obtained through a flash MW-assisted conversion process (2 min) of a cost-effective feedstock such as post-harvest tomato plants.[14]

Hierarchical SAPO-5 (labelled HierSAPO-5) was synthesized from a gel of molar composition: 1.0 Al : 0.93 P : 0.58 Si : 0.068 SDA_{meso} : 0.58 TEA : 44H_2O under hydrothermal conditions at 473 K for 60 h, using triethylamine (TEA) as the structure-directing agent (SDA) for the micropores, and a mixture of monosaccharides (see ESI for details†) from biomass as the mesoporogens (SDA_{meso}). For comparison, microporous SAPO-5 (labelled MicroSAPO-5) was also prepared under identical conditions, excluding the addition of mesoporogen. All the catalysts were calcined in air flow at 873 K for 16 h to remove the organic templates.

To confirm the phase-purity of the HierSAPO-5, XRD analysis was performed on the calcined material (Fig. S1†) and compared to XRD pattern of MicroSAPO-5; all the observable peaks are attributed to the AFI framework type, confirming that no significant secondary phases were present.

The textural properties of HierSAPO-5 were assessed by N_2 adsorption/desorption volumetric analysis at 77 K (Fig. 1). HierSAPO-5 exhibits type IV isotherm characteristic of a mesoporous material (Fig. 1) with mesopores of approximately 36

[a]*Department of Drug Science and Technology, Università degli Studi di Torino, V. Pietro Giuria 9, 10125 Torino, Italy*

[b]*Department of Science and Technological Innovation, Università del Piemonte Orientale, V. Teresa Michel 11, 15121 Alessandria, Italy. E-mail: enrica.gianotti@uniupo.it*

[c]*Department of Chemistry, Università degli Studi di Torino, V. Pietro Giuria 7, 10125 Torino, Italy*

† Electronic supplementary information (ESI) available. See DOI: 10.1039/d0ra06353c

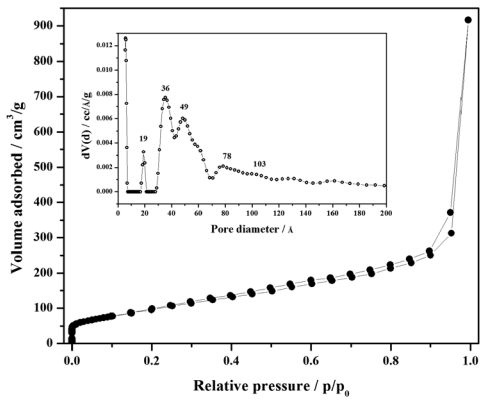

Fig. 1 N_2 adsorption/desorption isotherms at 77 K of hierarchical SAPO-5. Inset: the pore size distribution in the range of micropores and mesopores.

and 49 Å (Fig. 1, inset); in addition, micropores typical of AFI structure are also present. Significantly, with respect to MicroSAPO-5, the hierarchical catalyst exhibits substantial enhancements in mesopore volume (V_{meso}), total pore volume (V_{tot}) and mesopore surface area (S_{meso}) (Table 1). Volumetric data strongly support the successful preparation of HierSAPO-5 when MsB are used as mesoporogen, since there is experimental evidence for the coexistence of multiple levels of porosity.

Thermogravimetric and its derivative analyses (TGA/DTG) of the hierarchical and microporous SAPO-5 (Fig. S2†) revealed that, beside the weight loss due to physisorbed water (423 K), a weight loss at 673 K is present in both samples, attributed to the removal of TEA, *i.e.* the organic template for micropores. The amount of TEA in hierarchical catalyst is lower with respect to the microporous sample and in addition, a peak at *ca.* 453 K is visible due to the removal of the mesoporogen sugars.

The nature, strength and accessibility of the acid sites present in HierSAPO-5 was assessed by combined characterization using solid-state NMR and probe-FTIR[15] spectroscopy. The chemical environment of the framework atoms in hierarchical and microporous SAPO-5 was evaluated by ^{27}Al, ^{31}P, and ^{29}Si solid-state NMR spectroscopy (Fig. S3–S5†).

The ^{27}Al and ^{31}P MAS NMR spectra evidenced the presence of tetrahedrally-coordinated Al (at ~37.8 ppm, Fig. S3†) and P atoms (at −30.3 ppm, Fig. S4†), confirming strict alternation of Al and P at the T-positions of the AlPO-5 framework. In the ^{31}P MAS spectrum of the hierarchical material a shoulder downfield to the main peak is also present, due to P–OH defect sites.[18] On the other hand, the ^{29}Si NMR spectrum of MicroSAPO-5 exhibits signals at around −90, −95, −100, −105 and −110 ppm due to tetrahedral framework Si coordinated to four, three, two, one and zero Al atoms, respectively (Fig. S5†). ^{29}Si NMR spectrum of hierarchical material is dominated by contributions from Si(4Al) and Si(3Al) units while the formation of silicon islands (Si(0Al)) cannot be excluded.

The nature of the acid sites in HierSAPO-5 was investigated using ^{1}H MAS NMR and FTIR spectroscopy. ^{1}H MAS NMR spectra (Fig. 2) recorded using a spin-echo technique (a pulse sequence specially designed to avoid probe background signals) reveal two resonance peaks at around 3.5 and 4.5 ppm, associated with Brønsted Si(OH)Al sites (BAS1 and BAS2). In addition, signals due to P–OH/Al–OH (centred at 2.4 ppm) and isolated Si–OH (1.6 ppm) are also present.

In the FTIR spectra (Fig. S6†), SAPO-5 exhibits two well-separated bands at 3630 cm^{-1} and 3513 cm^{-1}. Both bands are associated with the Al(OH)Si Brønsted acid sites in different positions inside the AFI framework. The high frequency band is due to sites located in the 12-ring channels, whereas the band at 3513 cm^{-1} can be attributed to bridging OH located in the 6-ring channels. Defects ascribed to Si–OH (3745 cm^{-1}) or P–OH (3678 cm^{-1}) sites are also visible in the SAPO-5 catalyst.[16]

To discriminate the accessibility of the Brønsted acid sites, basic probe molecules with different kinetic diameters were adsorbed on HierSAPO-5 and followed by FTIR spectroscopy (Fig. 3). Firstly, to quantify the total amount of Brønsted acid sites, ammonia, that can enter both micro and mesopores due to its small dimension, was used.

Subsequently, pyridine and 2,4,6-trimethylpyridine (2,4,6-TMP or collidine) with larger kinetic diameters, were adsorbed.[12,17,18] The FTIR difference spectra of NH_3 (Fig. 3A), pyridine (Figure 3B) and 2,4,6-TMP (Fig. 3C) adsorbed on HierSAPO-5 at

Table 1 Textural properties of the hierarchical and microporous SAPO-5

	HierSAPO-5	MicroSAPO-5
S_{BET}/m^2 g^{-1}	370	270
S_{DFT}/m^2 g^{-1}	345	290
S_{micro}/m^2 g^{-1}	97	143
S_{meso}/m^2 g^{-1}	248	147
$V_{tot\ DFT}$/cm^3 g^{-1}	0.54	0.43
V_{micro}/cm^3 g^{-1}	0.025	0.044
V_{meso}/cm^3 g^{-1}	0.51	0.39

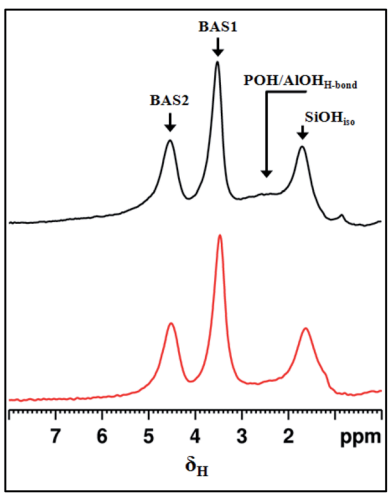

Fig. 2 ^{1}H spin-echo MAS NMR spectra of microporous (top) and hierarchical (bottom) SAPO-5. BAS: Brønsted acid sites, $SiOH_{iso}$: isolated silanols, $POH/AlOH_{H\text{-}bond}$: hydrogen bonded POH and AlOH sites.

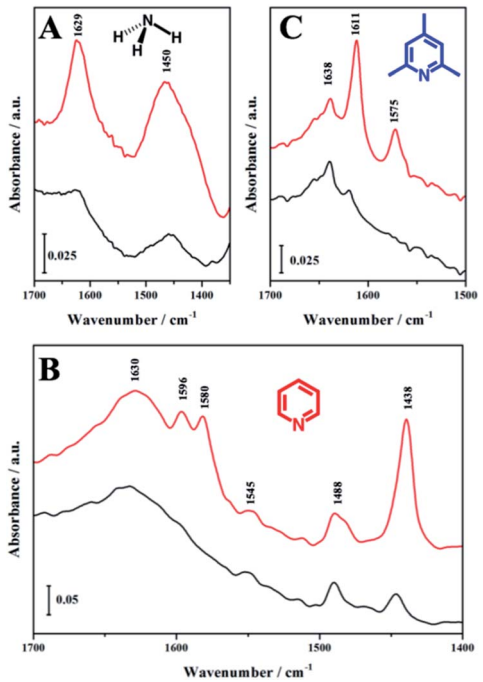

Fig. 3 FTIR difference spectra of NH_3 adsorption (A), of pyridine adsorption (B) and of 2,4,6-TMP adsorption (C) on HierSAPO-5. The spectra are shown before (red curve) and after outgassing the probe molecules at 298 K (black curve).

room temperature are reported in the low frequency region where the signals of protonated species are observed. Upon NH_3 adsorption at room temperature (Fig. 3A), a band at 1450 cm^{-1}, due to the asymmetric bending mode of NH_4^+ ions, indicates NH_3 protonation by Brønsted acid sites of the hierarchical catalyst. Furthermore, the bending mode of ammonia H-bonded to Si–OH or P–OH groups is detected at 1629 cm^{-1}. In the C–C ring-stretching region, pyridine adsorption (Fig. 3B) produces bands due to physisorbed pyridine (1580 ν_{8b} and 1438 ν_{19b} cm^{-1}), pyridine hydrogen-bonded to Si–OH or P–OH or on Lewis acid sites (1596 ν_{8b} and 1445 ν_{19b} cm^{-1}), and protonated species from interaction with strong Brønsted acid sites (1630 ν_{8a}, 1545 ν_{19b}, and 1488 ν_{19a} cm^{-1}). Finally, upon 2,4,6-TMP adsorption, bands at 1611 and 1575 cm^{-1} (owning to physisorbed 2,4,6-TMP) and a signal at 1638 cm^{-1} (owning to protonated 2,4,6-TMP) are formed.

The total number of accessible Brønsted acid sites (N) of HierSAPO-5 determined by using NH_3, pyridine and 2,4,6-TMP is reported in Table 2, together with the nature and the IR position of the bands of their protonated species. The accessibility factor (AF) is also calculated for pyridine derivatives. These data highlighted that only a small fraction of the total Brønsted acid sites are accessible to the bulkier probe molecules.

This newly designed catalyst was then applied for the MW-assisted conversion of glucose through Brønsted acidic catalysis. A well-known example hereof is the dehydration of sugars towards platform molecules like 5-HMF.[19]

This compound has been identified as among the top biomass-derived value-added chemicals,[20] since it is the starting material for biomass-based polymers, pharmaceuticals, agrochemicals, flavours and fragrances. It could be also a precursor for macro- and heterocycles, natural products and fuel components.[21] The peculiar properties of MW as a source of volumetric and selective dielectric heating have recently been exploited in the catalytic conversion of biomass, as they provide higher product yields and selectivity in reduced times.[22] Alternatively to aqueous media, non-aqueous systems have been proposed to prompt the MW-assisted dehydration to 5-HMF.[23] The catalytic activity of hierarchical SAPO-5 was thus tested either in water (Fig. 4A) or in the biomass-based solvent γ-

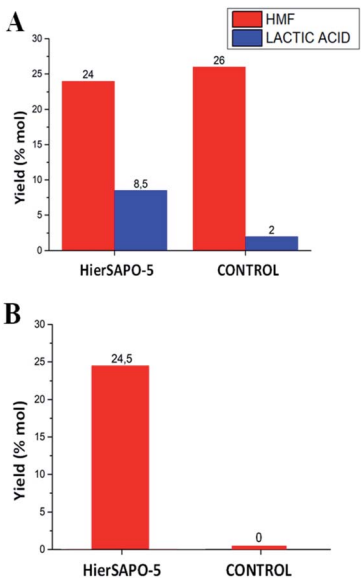

Fig. 4 MW-assisted glucose conversion in water (A) and GVL (B) at 443 K for 20 minutes.

Table 2 The concentration of accessible Brønsted acid sites (N) in hierarchical SAPO-5

Probe molecules	Protonated species	Position of IR bands of protonated species [cm^{-1}]	N [μmol g^{-1}]	AF
NH_3	NH_4^{+a}	1450 (δ_{asym})	40.9	1
Pyridine	PyH^{+b}	1545 (ν_{19b})	13.7	0.34
2,4,6-TMP	2,4,6-$TMPH^{+c}$	1638 (ν_{8a})	0.9	0.021

[a] $\varepsilon = 0.147$ cm^2 μmol^{-1}. [b] $\varepsilon = 0.06$ cm^2 μmol^{-1}. [c] $\varepsilon = 0.62$ cm^2 μmol^{-1}.

valerolactone (GVL, Fig. 4B), which can reduce the side reactions and thereby increases the selectivity toward 5-HMF. The reactions were performed at 443 K as this was the temperature providing the best yields in similar systems.[24] The optimized conditions involved a reaction time of 20 minutes.

Indeed, a time decrease leads to a lower conversion, while longer times provide lower yields owing to a partial product degradation into unidentified soluble polymers and humines (data not shown). A reaction without the addition of HierSAPO-5 was also performed in the same conditions, as the control. As reported in Fig. 4A, using water as the solvent, the reaction proceeds with almost the same yields of 5-HMF either with or without the catalyst. However, the zeolite catalysed the formation of higher yields of lactic acid. It is now well established that glucose isomerization to fructose takes place on Lewis acid sites, and the dehydration step requires Brønsted acid sites.[4] Basing on the catalytic results, *i.e.* on the obtained yields of 5-HMF and lactic acid, it can be hypothesized that in water only the small amount Lewis acid sites (detected by FTIR) play a role in the product formation, whilst the Brønsted sites may be reasonably involved in strong interaction with water. Indeed, there is no contribution by the HierSAPO-5 catalyst in the 5-HMF yield (being the same as in the control experiment), which is due only to the hydrothermal conversion under MW irradiation. On the contrary, lactic acid is formed by the conversion of fructose to glyceraldehyde and dihydroxyacetone by a retro-aldol reaction involving the C–C bond cleavage (Fig. 5, Path 2), which can be favoured by Lewis acid sites.[25] When performing the reaction in GVL, no glucose conversion was observed in the absence of the catalyst (Fig. 4B). In addition, lactic acid was not produced under these conditions.

Therefore, it is very much worth noting that the solvent mediates glucose conversion to 5-HMF through a synergism with HierSAPO-5, prompting the action of both Lewis and Brønsted acid sites according to Path 1 (Fig. 5).

These preliminary results pointed out the synergism between the solvent and the HierSAPO-5 catalyst in the selectivity of glucose conversion, despite the yields to 5-HMF still need to be improved. In addition, MicroSAPO-5 was also tested in the same condition and the yield to 5-HMF achieved was almost comparable to HierSAPO-5, due to the small dimension of glucose substrate. However, XRD measurements on both MicroSAPO-5 and HierSAPO-5 samples before and after reaction in GVL (Fig. S7†) revealed that the introduction of mesopores guaranteed an improved structural stability of the HierSAPO-5 catalyst with respect to MicroSAPO-5 and a better diffusion of reactants, opening the door to the design of robust heterogeneous catalysts for biomass conversion.

Indeed, other SAPOs systems[24,26] gave good results, however the catalytic test were performed using different reaction media.

In summary, a new hierarchical SAPO-5 was synthesised using a mixture of MsB coming from the flash conversion of waste biomass. This new catalyst was fully characterized and tested in the MW-assisted glucose conversion. Full selectivity toward 5-HMF was achieved using GVL as the solvent. This is a sustainable solvent, as it is biomass-derived, nontoxic and biodegradable. Furthermore, the use of MW further prompts the sustainability of the process by reducing the reaction times, compared to literature experiments.

In perspective, the sugars obtained from biomass conversion can be used both as templates and as substrates for the synthesis of high value added products through the sustainable MW-assisted processes.

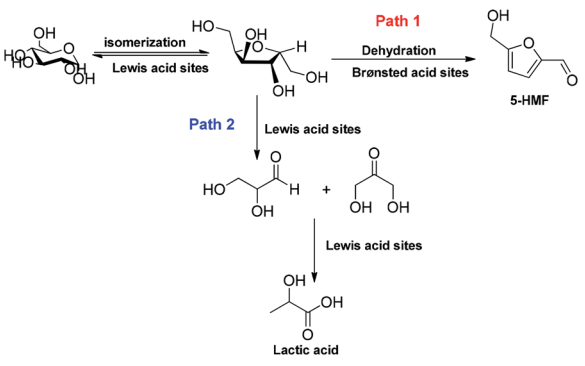

Fig. 5 Proposed mechanisms for the influence of Brønsted and Lewis acid sites in product formation.

Conflicts of interest

There are no conflicts to declare.

Acknowledgements

The project leading to these results has received funding from the European Union's Horizon 2020 research and innovation program under grant agreement no. 720783 – MULTI2HYCAT and from the University of Turin, Italy (Ricerca locale 2020).

References

1 J. Cejka, G. Centi, J. Perez-Pariente and W. J. Roth, *Catal. Today*, 2012, **179**, 2–15.
2 *Zeolites and Catalysis: Synthesis, Reactions and Applications*, ed. J. Cejka, A. Corma and S. Zones, Wiley-VCH, Weinheim, 2010, vol. 2.
3 D. P. Serrano, J. A. Melero, G. Morales, J. Iglesias and P. Pizarro, *Catal. Rev.: Sci. Eng.*, 2018, **60**, 1–70.
4 T. Ennaert, J. Van Aelst, J. Dijkmans, R. De Clercq, W. Schutyser, M. Dusselier, D. Verboekend and B. F. Sels, *Chem. Soc. Rev.*, 2016, **45**(3), 584–611.
5 P. Sudarsanam, E. Peeters, E. V. Makshina, V. I. Parvulescu and B. F. Sels, *Chem. Soc. Rev.*, 2019, **48**, 2366–2421.
6 X. Zhu, J. P. Hofmann, B. Mezari, N. Kosinov, L. Wu, Q. Qian, B. M. Weckhuysen, S. Asahina, J. Ruiz-Martinez and E. J. M. Hensen, *ACS Catal.*, 2016, **6**, 2163–2177.
7 W. Schwieger, A. G. Machoke, T. Weissenberger, A. Inayat, T. Selvam, M. Klumpp and A. Inayat, *Chem. Soc. Rev.*, 2016, **45**, 3353–3376.
8 M. Moliner, C. Martínez and A. Corma, *Angew. Chem., Int. Ed.*, 2015, **54**, 3560–3579.
9 M. Hartmanna and L. Kevan, *Chem. Rev.*, 1999, **99**, 635–664.

10 E. Gianotti, M. Manzoli, M. E. Potter, V. N. Shetti, D. Sun, J. Paterson, T. M. Mezza, A. Levy and R. Raja, *Chem. Sci.*, 2014, **5**, 1810–1819.
11 E. M. Flanigen, B. M. Lok, R. L. Patton and S. T. Wilson, *Stud. Surf. Sci. Catal.*, 1986, **28**, 103–112.
12 I. Miletto, C. Ivaldi, G. Paul, S. Chapman, L. Marchese, R. Raja and E. Gianotti, *ChemistryOpen*, 2018, **7**, 297–301.
13 D. Nandan, S. K. Saxena and N. Viswanadham, *J. Mater. Chem. A*, 2014, **2**, 1054–1059.
14 S. Tabasso, E. Montoneri, D. Carnaroglio, M. Caporaso and G. Cravotto, *Green Chem.*, 2014, **16**(1), 73–76.
15 G. Paul, C. Bisio, I. Braschi, M. Cossi, G. Gatti, E. Gianotti and L. Marchese, *Chem. Soc. Rev.*, 2018, **47**, 5684–5739.
16 M. E. Potter, M. E. Cholerton, J. Kezina, R. Bounds, M. Carravetta, M. Manzoli, E. Gianotti, M. Lefenfeld and R. Raja, *ACS Catal.*, 2014, **4**, 4161–4169.
17 F. Thibault-Starzyk, I. Stan, S. Abellu, A. Bonilla, K. Thomas, C. Fernandez, J.-P. Gilson and J. Perez-Ramirez, *J. Catal.*, 2009, **264**, 11–14.
18 I. Miletto, G. Paul, S. Chapman, G. Gatti, L. Marchese, R. Raja and E. Gianotti, *Chem.–Eur. J.*, 2017, **23**, 9952–9961.
19 T. Ennaert, J. Van Aelst, J. Dijkmans, R. De Clercq, W. Schutyser, M. Dusselier, D. Verboekend and B. F. Sels, *Chem. Soc. Rev.*, 2016, **45**, 584–611.
20 J. J. Bozell and G. R. Petersen, *Green Chem.*, 2010, **12**, 539–554.
21 L. T. Mika, E. Cséfalvay and Á. Németh, *Chem. Rev.*, 2018, **118**, 505–613.
22 E. Calcio Gaudino, G. Cravotto, M. Manzoli and S. Tabasso, *Green Chem.*, 2019, **21**, 1202–1245.
23 X. Jia, I. K. M. Yu, D. C. W. Tsang and A. C. K. Yip, *Microporous Mesoporous Mater.*, 2019, **284**, 43–52.
24 L. Zhang, G. Xi, Z. Chen, Z. Qi and X. Wang, *Chem. Eng. J.*, 2017, **307**, 877–883.
25 L. Yang, X. Yang, E. Tian, V. Vattipalli, W. Fan and H. Lin, *J. Catal.*, 2016, **333**, 207–216.
26 P. Bhaumik and P. L. Dhepe, *RSC Adv.*, 2013, **3**, 17156.

